Available online at www.sciencedirect.com
SCIENCE DIRECT®
ELSEVIER
European Journal of Mechanics B/Fluids 23 (2004) 617–632
EUROPEAN JOURNAL OF MECHANICS B/FLUIDS

On the pressure oscillations inside a deep cavity excited by a grazing airflow

P. Hémon [a], F. Santi [b], X. Amandolèse [c]

[a] *Hydrodynamics laboratory, LadHyX, École polytechnique – CNRS, 91128 Palaiseau cedex, France*
[b] *CNAM, Department of Mathematics, 292, rue Saint-Martin, 75141 Paris cedex 03, France*
[c] *Institut aérotechnique/CNAM, 15, rue Marat, 78210 Saint-Cyr l'École, France*

Received 4 March 2003; accepted 10 September 2003

Available online 3 December 2003

Abstract

An experimental and theoretical study of the pressure oscillations generated by the flow over a deep cavity is presented. Such a configuration, which is akin to a Helmholtz resonator, arises in many applications, for instance when a window or the sunroof of an automobile remains open. The linear resonator model is fully validated by experiments. The linear stability characteristics of the free shear layer in the neck of the cavity are retrieved from neck wall pressure measurements. An efficient sound reduction scheme is proposed, which is based on the use of piezo-electric actuators placed upstream of the neck. These elements act as small discrete flaps which force the shear layer in the neck to oscillate at a frequency distinct from the cavity resonance frequency. A quasi complete attenuation of the peak pressure may then be achieved. The classical linear stability analysis of the free shear layer is successful in accounting for the experimental observations and it leads to the identification of the physical mechanism responsible for the efficiency of the sound reduction scheme. Moreover linear stability theory yields limitations to the efficiency of the technique in the form of an energy criterion involving the Strouhal number.

Keywords: Cavity; Shear layer; Aeroacoustics; Instability

List of notations

A_c	Neck section (m^2)
c	Sound velocity (m/s)
f_c	Frequency of the shear layer instability (Hz)
f_v	Resonance frequency of the cavity (Hz)
H	Effective thickness of the neck (m), $H = H_c + 2H'$
H_c	Thickness of the neck (m)
H_v	Height of the cavity (m)
H'	Added thickness of the neck (m)
k	Wave number (complex)
$L,\ L_v$	Length of the neck, of the cavity (m)
L_0	Reference thickness of the shear layer (m)
M	Mach number, $M = U_1/c$

E-mail address: pascal.hemon@ladhyx.polytechnique.fr (P. Hémon).

0997-7546/$ – see front matter
doi:10.1016/j.euromechflu.2003.09.005

p_c, p_v, p_e Acoustic pressures in the neck, in the cavity and outside the cavity
p_1, p_2, p_3 Wall pressures around the neck: backward face, forward face and upstream
St Strouhal number, $St = fL_0/U_1$
U Velocity (m/s)
U_c Convection velocity (m/s)
U_1 Upper free-stream velocity of the shear layer (m/s)
U_2 Lower free-stream velocity of the shear layer (m/s)
V Volume of the cavity (m^3)
W_c, W_v Spanwise width of the neck, of the cavity (m)
x, z Streamwise and wall normal coordinates
χ Relative energy of forcing
δ_1, δ_2 Boundary layer displacement and momentum thicknesses (m)
δ_ω Shear layer vorticity thickness (m) $\delta_\omega = 2L_0$
γ Empirical parameter in Rossiter's formula
η_r Reduced damping of the resonator
ρ Air density (kg/m^3)
ω Angular frequency (rad/s)
ω_c Angular frequency of the shear layer (rad/s), $\omega_c = 2\pi f_c$
ω_r Angular frequency of the resonator (rad/s), $\omega_r = 2\pi f_v$

1. Introduction

1.1. Pressure oscillations in flow over cavities

Pressure oscillations generated by the flow over cavities have been widely studied in the past due to their importance in aeronautics. In the present paper, we study this problem in the context of car vehicles which exhibit low-frequency oscillations when windows or sunroofs are opened. The improvement of the airtightness, combined with the increasing volume of the passenger compartment, lead to a higher sensitivity to self-sustained interior pressure oscillations. In most cases, the phenomenon causes nausea and headache to the passengers and the driver. Automobile manufacturers must therefore devise technical solutions to prevent these oscillations.

In practice, the problem can be reduced to the deep cavity configuration sketched in Fig. 1. As shown by Kang et al. [1] the passenger compartment has however a more complex shape leading to a number of acoustic modes which may become active in the response.

There exists a large number of publications concerning cavity pressure oscillations: many of them are mainly interested in the characteristic frequencies of oscillations, for instance [2–5]. The effect of the cavity geometry has also been studied: the depth of the cavity by East [6], the neck geometry by Panton [7], and recently the aspect ratio of a rectangular neck by Disimile et al. [8]. A scaled model of a vehicle has been considered in [9]. It shows how difficult it is to suppress the oscillations without directly acting on the mean flow characteristics, for instance by using a spoiler.

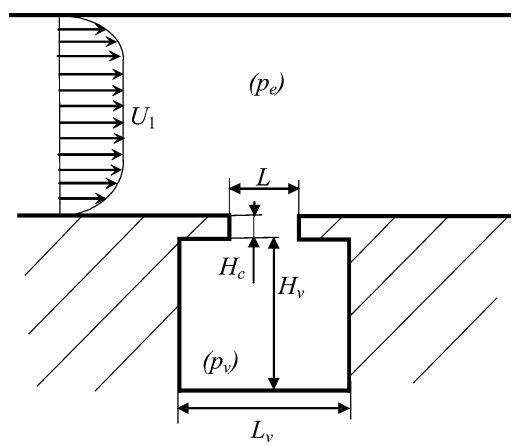

Fig. 1. Cross-sectional view defining the geometrical parameters.

The reduction of the pressure level in the cavity may also be achieved in a different way. It consists in applying an unsteady pressure field inside the cavity by means of a loudspeaker and implementing an active control method [10]. One encounters also actuators made of small pulsed jets near the trailing-edge. Another technique consists in mounting an active spoiler on the trailing edge of the cavity neck, using loudspeakers [11] or using piezo-electric materials as actuators [12,13].

The latter was employed also by Amandolèse et al. [14] and the present paper is an extension of these experimental results in order to more satisfactorily explain the physical behaviour of the system. The study is organized as follows. First, the origin of the oscillations is examined from a hydrodynamic stability point of view. The experimental set up and conditions are described (Section 2) and measurements are made in order to validate a model of the Helmholtz resonator (Section 3). The excitation term for this resonator, provided by the neck pressure, is approached within the context of linear stability theory (Section 4). A sound reduction scheme is finally presented and discussed in Section 5.

1.2. From free shear layers to cavity necks

As will be seen hereafter, the mean flow field in the neck of the cavity, for instance in the Helmholtz resonator of Fig. 1, is similar to the mean velocity profile of a free shear layer. The unstable behaviour of this fundamental base flow constitutes therefore an essential ingredient in understanding the origin of the pressure oscillations. The linear instability properties of free shear layers have been studied by Michalke, for the temporal [15] and spatial [16] cases by using the hyperbolic tangent velocity profile as an approximation.

A generalization was then proposed by Monkewitz and Huerre [17,18]. In the latter, it is demonstrated that the mixing layer with a small velocity ratio, which is our case, is subjected to a convective instability, i.e. instability waves are spatially growing and advected along the streamwise direction. In the experimental study of Ho and Huang [19], it was demonstrated that vortex merging and the associated subharmonic instability constituted the main mechanism for the streamwise growth of mixing layers. This pairing phenomenon occurs at given locations in the streamwise direction and it coincides with an increase of the local spreading rate.

However, in the case of a cavity, the streamwise direction is bounded by the edges of the neck, which leads to an additional perturbation generated by the periodic impingement of the vortices. This results in the generation of self-sustained shear layer oscillations, the frequency of which is related to the distance between the upstream and downstream edges [20]. This phenomenon has been found in a wide range of flow situations as reviewed by Rockwell [21]. It is roughly explained by a feed-back mechanism in which the impingement of a vortex creates an acoustic pulse travelling upstream and thus triggering the shedding of a new synchronized vortex.

When a cavity is flush mounted, interactions between these oscillations and the acoustic modes of the cavity become possible, leading to high level tones, as described for instance by Meissner [22].

2. Experimental techniques and setup

The cavity models are mounted in a small acoustic wind tunnel of the Institut Aérotechnique which generates low noise airflow. An original feature of the facility is that it allows measurements of the external acoustic pressure p_e for a given range of frequencies [80–660 Hz] even when the wind is blowing: this kind of measurement is performed by plane wave intensimetry which is limited to frequencies lower than 660 Hz due the size of the tunnel section. The pressure p_v in the cavity is measured by a microphone (type 4193 provided by B & K).

The wall pressures around the neck, p_1, p_2 and p_3, as specified in Fig. 2, are measured with flush-mounted miniature piezo-resistive microphones (type 8507C-2 provided by Endevco) which yield the mean and the fluctuating pressures. The sensitive region of these probes is a small circle 2 mm in diameter which is well suited to small models. The vertical location for p_1 and p_2 is $z = -1.15$ mm and the streamwise location for p_3 is $x = -7$ mm.

A data acquisition PAK system provided by Müller-BBM is used together with the measurement hardware based on the VXI standard. The acquisition card is a 16 bits A/D converter equipped with direct signal processors for Fast Fourier Transform measurements. The frequency resolution is chosen to be 0.18 Hz. The acoustic pressure accuracy is typically 1dB, and 5% for the mean wall pressures. The reference free-stream velocity is measured with an accuracy of around 1%.

Pressure measurements are supplemented with hot wire velocity measurements. Boundary layer probes (type P15 provided by Dantec) are used. The constant temperature anemometer is calibrated using a standard calibration nozzle and a nonlinear fitting curve with a resulting accuracy less than 5% maximum for the very low velocities. Acquisition and numerical processing were also made using the PAK system. The probes are mounted on a small vertical displacement trail which has a position resolution of 0.1 mm.

Two models of the cavity have been flush-mounted in a rectangular closed test section 260 mm high and 300 mm wide. The first two transverse acoustic modes of the tunnel are then 670 and 580 Hz respectively. No interactions were expected to occur

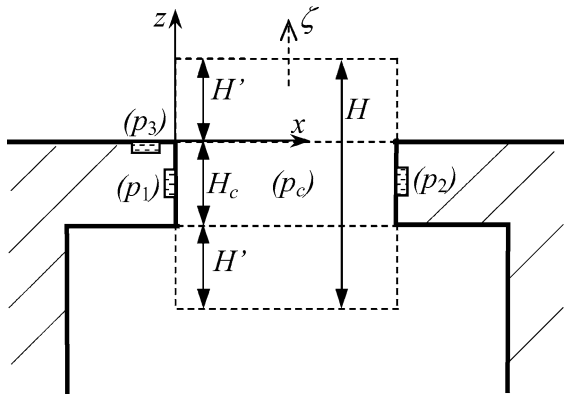

Fig. 2. Detail of the neck cross-sectional view.

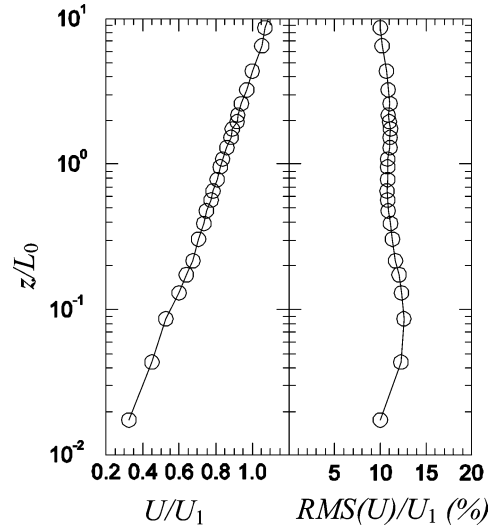

Fig. 3. Boundary layer profile $0.25L$ upstream of the neck.

Table 1
Cavity dimensions

	Cavity A	Cavity B
L_v (m)	0.100	0.0072
H_v (m)	0.195	0.195
W_v (m)	0.200	0.200
V (m^3)	0.0039	0.0028

Table 2
Neck dimensions and characteristics

L (m)	0.020
H_c (m)	0.005
W_c (m)	0.200
H' (m)	0.0203
A_c (m^2)	0.0040

with the cavity oscillations which have much lower frequencies. However, one can notice that a resonance may be observed (cavity A peak 2 in Fig. 4). Two anechoic terminations are also mounted at the extremities of the test section. This ensure that there is no significant reflexive longitudinal wave that could propagate along the tunnel, which was verified by intensimetry.

The dimensions of the cavity models are given in Tables 1 and 2. The neck is identical for both deep cavities with a height $H_v = 10L$. All these dimensions have been chosen a priori in order to obtain a resonance frequency within the intensimetry measurement range of the setup for a wind velocity between 10 and 25 m/s.

The incoming boundary layer profile is measured in detail: the mean and the root-mean-square (RMS) velocities are given in Fig. 3 in nondimensional variables scaled with respect to the upper velocity of the shear layer U_1 and the reference height L_0. This height is characteristic of the velocity vertical gradient inside the neck, which is essential in the excitation mechanism and will be detailed later on. The mean velocity profile outside the viscous sub-layer can be fitted by a logarithmic profile, which is a typical characteristic of a fully developed, equilibrium, turbulent boundary layer, with zero pressure gradient. The resulting displacement and momentum thicknesses are $\delta_1 = 4.5$ mm and $\delta_2 = 3.6$ mm.

3. The Helmholtz resonator

The purpose of this section is to study a simplified system representation of the passenger compartment in a car vehicle. Typically such a configuration may be considered as a Helmholtz resonator. We first describe the analytical model for this system, with the internal acoustic pressure p_v as the main reference variable. In a second step, the experimental validation of the model is presented.

3.1. Basic equation

The Helmholtz resonator has been widely described from an acoustical point of view, notably by Bruneau [23]. Starting from the geometrical parameters shown in Fig. 1, the displacement ζ of the air layer in the neck section follows the basic equation

$$\rho A_c H\ddot{\zeta} + \rho c A_c(2R_0 + R_1 + \Gamma H_c)\dot{\zeta} + \rho c^2 \frac{A_c^2}{V}\zeta = \xi A_c p_c, \tag{1}$$

where the acoustic pressure p_c in the neck (spatial mean) acts as the excitation force for the resonator, ξ is a dimensionless coefficient to be determined and R_0, R_1 and Γ are damping parameters detailed below. The assumption is made that the acoustic wavelength is larger than the geometrical dimensions of the system under consideration, so that the resonator is acoustically compact.

According to the linear acoustic approximation for a perfect gas, the displacement of the air layer in the neck is linked to the acoustic pressure inside the cavity via the relation

$$\zeta = \frac{V}{A_c \rho c^2} p_v. \tag{2}$$

By substituting (2) into (1) we obtain the basic equation for the cavity pressure

$$\frac{VH}{A_c c^2} \ddot{p}_v + (2R_0 + R_1 + \Gamma H_c) \frac{V}{A_c c} \dot{p}_v + p_v = \xi p_c. \tag{3}$$

In this expression, H is the effective thickness of the air which oscillates in the neck. It is composed of the thickness of the neck H_c increased by the thicknesses H' of the air layers which are entrained, as sketched in Fig. 2. There exists a number of expressions which give these added thicknesses, especially for circular holes. In the present case, the shape of the aperture is rectangular, close to a slit and the usual expression $H' = 0.4\sqrt{A_c}$ is not applicable. For noncircular holes, Crighton et al. [24] and references therein, provide the relation

$$H' = 0.85 A_c^{0.75} / \sqrt{l_c}, \tag{4}$$

where l_c is the perimeter of the aperture.

The term R_0 represents radiation damping due to the power lost by the resonator to the surrounding medium and to the cavity volume [23]. It is proportional to the square of the angular frequency and given by

$$R_0 = \frac{\omega^2 A_c}{2\pi c^2}. \tag{5}$$

The term R_1 in (3) represents the power lost due to the cavity wall impedance. The last damping term Γ is a dissipation factor due to viscous effects along the walls of the neck. Using the analytical expression provided by Bruneau [23], it is found that these two damping terms are numerically much smaller than the damping due to radiation through the neck and they can be neglected. Finally the basic equation of the resonator becomes

$$\ddot{p}_v + \frac{\omega^2 A_c}{\pi (H_c + 2H') c} \dot{p}_v + \frac{c^2 A_c}{V(H_c + 2H')} p_v = \xi \frac{c^2 A_c}{V(H_c + 2H')} p_c. \tag{6}$$

Introducing the resonator eigenfrequency

$$\omega_r = c \sqrt{\frac{A_c}{V(H_c + 2H')}}, \tag{7}$$

and the reduced damping

$$\eta_r = \omega^2 \omega_r \frac{V}{2\pi c^3}, \tag{8}$$

Eq. (6) reduces to

$$\ddot{p}_v + 2\eta_r \omega_r \dot{p}_v + \omega_r^2 p_v = \xi \omega_r^2 p_c. \tag{9}$$

The final form (9) is similar to a standard damped mechanical oscillator excited by the shear layer instability in the neck.

3.2. Comparison with experiments

3.2.1. Frequency and damping without flow

The resonance frequency ω_r and the reduced damping η_r are measured without wind by using an acoustic source delivering a (pseudo) white noise in the test section. The parameters of the resonator can be retrieved by measuring the transfer function (modulus and phase angle φ) between the external pressure p_e and the cavity pressure p_v. In fact the resonator equation (9) should be rewritten in the form

$$\ddot{p}_v + 2\eta_r \omega_r \dot{p}_v + \omega_r^2 (p_v - p_e) = 0, \tag{10}$$

Table 3
Cavity A resonance frequencies and damping without flow

	Theoretical	Experimental
f (Hz)	259 ± 1	268 ± 2
η_r (%)	6.8 ± 0.1	2.05 ± 0.15

where the external pressure is assumed to be of the form

$$p_e = \alpha p_v + \beta \dot{p}_v. \tag{11}$$

Upon using Fourier transforms, it is easy to show from (11) that

$$\alpha = \frac{\cos\varphi}{|p_v/p_e|} \quad \text{and} \quad \beta = \frac{-\sin\varphi}{\omega|p_v/p_e|}. \tag{12}$$

The first coefficient α should be regarded as an added stiffness, and the second β as an added damping. The latter can be rewritten as a reduced damping, leading to

$$\eta_{\text{exp}} = \frac{-\sin\varphi}{2|p_v/p_e|}\frac{\omega_r}{\omega}, \tag{13}$$

which can then be compared with the theoretical value (8). At resonance, the system has to be in equilibrium, i.e. at a zero balance of energy over one period, which implies $\eta_{\text{exp}} = \eta_r$ and $\omega = \omega_r$.

The comparison between experimental and theoretical results is given in Table 3 for cavity A, where the specified dispersion in the numerical values is due to temperature variations during the tests (between 20 °C and 25 °C). The phase angle at the specified resonance frequency was measured to be exactly $-90°$, as expected for such an oscillator.

The comparison between experiments and theory is very favourable for the resonance frequency, (3.4% difference), showing the reliability of the neck thickness correction based on Eq. (4). The same behaviour was found for cavity B, with a theoretical frequency of 305 Hz, against 302 Hz for the experiments.

However, the measured damping does not agree so well with the theoretical value. One explanation might be the effect of confinement due to the closed test section, which constitutes the main difference with the assumptions underlying the theoretical expression (5) for which an infinite medium above the cavity neck is assumed. In the following, the experimental value will be used.

3.2.2. Results in presence of grazing flow

The measured frequency and the cavity pressure level p_v are given in Fig. 4 versus the free-stream velocity U_1. The linear evolution of the frequency will be discussed later: the purpose of this section is to present the different kinds of resonance peaks which are observed.

For cavity A, the presence of two peaks has to be accounted for. The first one occurs around the eigenfrequency of the Helmholtz resonator and it is due to resonance with the impinging shear layer. The resonance frequency, at which the pressure level is maximum, is modified by the flow and decreases from 268 Hz (see Table 3) to 262 Hz (see Fig. 4). The acoustic power generated, measured by intensimetry reaches 83 dB (referred to 10^{-12} W) at resonance, which is considerable for a single tone.

The second peak is however more complex and should be considered as an experimental artefact because it is linked to a resonance of a first harmonic of the shear layer (2×290 Hz) with an acoustic transverse mode of the test section (580 Hz). This interpretation was experimentally verified once by modifying temporarily the transverse dimension of the test section, thereby modifying the related frequency. As expected, the measurements then showed the suppression of this peak.

The purpose of this paper is focused on the first of these two peaks, even if the experimental results will consider both. Similar duct – cavity resonances have been experimentally studied by Amandolèse et al. [25].

For cavity B, the previous two resonances are not well separated in frequency and produce a single but wider peak. The pressure level is also much higher, which is attributed to a resonance involving three systems: the shear layer, the cavity and the test section.

3.2.3. Added damping and stiffness in the presence of flow

The transfer function p_v/p_e was measured for both cavities and the two peaks which appeared in the response. This is significant only when the coherence function is close to unity and the reported results satisfy this condition. Far from the resonance points, the coherence vanishes and the measurements are not possible.

The added damping η and stiffness α are given in Fig. 5 versus the dimensionless frequency, i.e. the Strouhal number, defined by $St = fL_0/U_1$. The reference length L_0 corresponding to the height of the shear layer in the cavity neck will be detailed

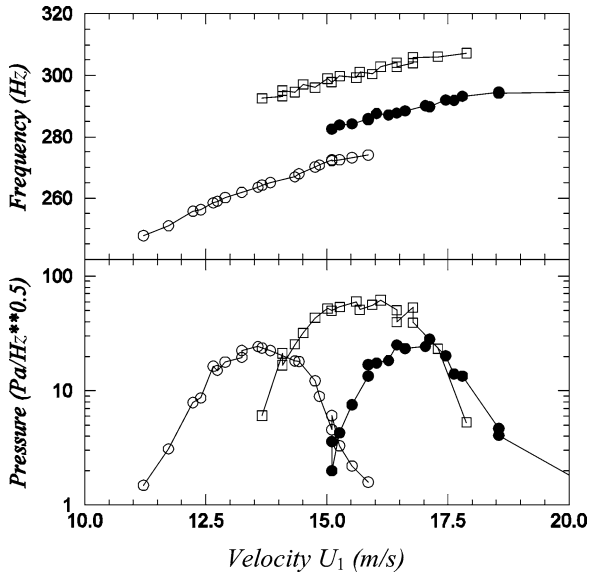

Fig. 4. Cavity pressure level p_v and frequency versus free-stream velocity U_1: ○, cavity A peak 1; ●, cavity A peak 2; □, cavity B.

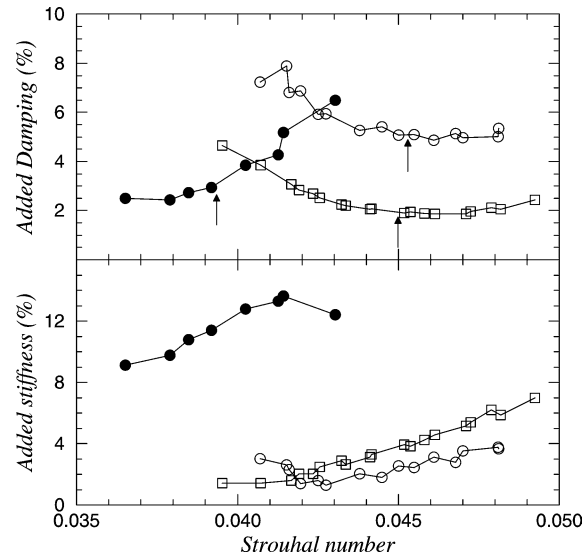

Fig. 5. Reduced added damping η and added stiffness α versus Strouhal number St: ○, cavity A peak 1; ●, cavity A peak 2; □, cavity B.

later. The documented damping is the additional term due to the flow, obtained by subtracting the resonator damping from the total damping. The resonance points have been indicated with an arrow. One can observe a similar behaviour of the cavity A peak 1 (cavity-shear layer resonance) with the cavity B peak. Particularly, the damping is at a minimum when resonance occurs, which is not the case for the test section resonance.

The difference between the test section-shear layer resonance and the cavity-shear layer resonance is more obvious for the added stiffness, which is negligible for the cavity-shear layer resonance, whereas it reaches more than 12% for its test section – shear layer counterpart.

3.2.4. Excitation term

The knowledge of the excitation term is not trivial, since it should be considered as the streamwise mean of the unsteady pressure along the neck. The wall acoustic pressures p_1 and p_2, defined in Fig. 2, represent the limiting range of this excitation pressure. Their dimensionless levels are given in Fig. 6 together with the upstream wall pressure p_3. The phase angle pertaining to p_1 is also given for later use. The displayed results extracted from the PSD are those for which the coherence function between p_1 and p_2 and between p_1 and p_3 is unity at the corresponding frequency. They are therefore within the lock-in region.

It is interesting to observe that the pressure ratios are quasi-constant with Strouhal number in the explored range. The upstream wall pressure p_3 shows a particularly strong coupling with the cavity pressure p_v which is logical for the present very low Mach number flow, as already observed for instance by Graf and Durgin [26].

At resonance, the transfer function of the linear Helmholtz oscillator (9) leads to an estimation of the value of ξ as

$$\xi = 2\eta_{\text{exp}} \left| \frac{p_v}{\langle p_c \rangle} \right|. \tag{14}$$

We will see in the next section that the neck pressure evolution along the stream takes an exponential form, which through a spatial integration yields the spatial mean value $\langle p_c \rangle$. This leads to the result $\xi = 0.0637$.

The last unknown quantity in the model (9) of the Helmholtz resonator excited by a grazing flow is the pressure p_c. This pressure is generated by the grazing flow over the neck thereby creating a shear layer which oscillates via a self-sustaining mechanism. The next section presents the application of the linear stability theory of mixing layers to the problem at hand. The analysis of the experimental results will further validate the concepts.

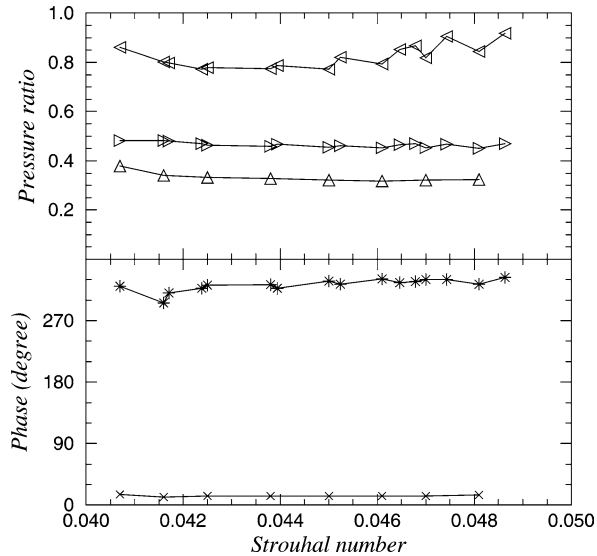

Fig. 6. Neck wall pressures versus Strouhal number St: ▷, p_1/p_v; ◁, p_2/p_v; Δ, p_3/p_v; *, $\varphi_{2/1}$; ×, $\varphi_{3/1}$.

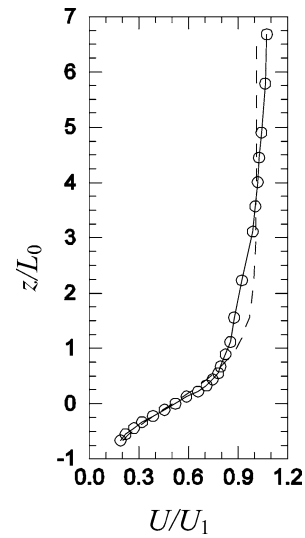

Fig. 7. Shear layer mean velocity profile at $x = 0.5L$: ---, hyperbolic-tangent; ○, measurements.

4. Shear layer instability

4.1. Theoretical background

This section is devoted to the application of hydrodynamic stability theory in order to describe the behaviour of the pressure in the neck. It is mainly based upon the work of Michalke [15,16], which is generalized in [17] and reviewed more recently by Huerre and Rossi [27]. Our interest lies in disturbances travelling and growing in the mean flow direction along the neck length. Thus one has to deal with the spatial problem which was studied by Michalke [16]. The results can be compared with the experiments, especially in order to validate the control concept proposed in Section 5. The present study is concerned with cavity A peak 1, i.e. the resonance between the Helmholtz resonator and the shear layer.

4.1.1. Reference quantities and hyperbolic tangent velocity profile

The mean flow characteristics of the mixing layer inside the neck provide the velocity scale and the length scale which are essential in the determination of the instability characteristics. The mean velocity profile is measured at mid-length of the neck with a hot wire probe and it is given in Fig. 7. Due to the small dimension of the set-up, only one streamwise position could be explored without perturbing the flow by the intrusion of the probe. The mid-length position is considered as a good compromise to represent the evolution of the shear layer velocity profile in the neck.

The mean velocity profile is fitted as in [17] by the hyperbolic-tangent profile,

$$U = U_1\big[1 + R\tanh(z/L_0)\big]/2, \tag{15}$$

where the velocity ratio is by definition

$$R = (U_1 - U_2)/(U_1 + U_2). \tag{16}$$

Nonlinear best fitting of the experimental curve leads $R = 1.02$. The velocity ratio R may effectively be taken to be unity as in Michalke [16]. This means that the lower shear layer velocity U_2 is zero. It must be noted that the profile in the upper region does not fit well with the hyperbolic tangent velocity profile, which is due to the internal flow characteristics. The mixing region, which is fundamental in the problem at hand, is however well represented.

At $0.5L$ of the neck, the best nonlinear fit of the experimental profile leads $L_0 = 2.3$ mm and $U_1 = 13.24$ m/s. Note that the chosen reference length L_0 is just the vorticity thickness $\delta_\omega = (U_1 - U_2)/(\partial U/\partial z)_{\max}$ (with $U_2 = 0$ in the present case) divided by 2 [17]. By using the dimensionless quantities $\tilde{z} = z/L_0$ and $\widetilde{U} = U/U_1$, the velocity profile reduces to

$$\widetilde{U}(\tilde{z}) = [1 + \tanh\tilde{z}]/2. \tag{17}$$

4.1.2. Stability analysis

We give a brief summary of the analysis of Michalke [16]. We focus the study on the flow in the neighbourhood of the cavity neck which is supposed two-dimensional and parallel. The influence of the feed-back and the coupling with the cavity volume is not taken into account in this analysis.

The velocity and pressure fields are decomposed into a mean and an unsteady part according to

$$\begin{aligned} &U(x,z,t) = U(z)e_x + u(x,z,t)e_x + v(x,z,t)e_z, \\ &P(x,z,t) = P_0 + p(x,z,t). \end{aligned} \tag{18}$$

For simplification, the symbol $\sim$ denoting dimensionless quantities is omitted. The mean velocity is given by the hyperbolic tangent profile (17) and P_0 is a constant pressure. Assuming small fluctuations, the problem is analysed within the linearized inviscid incompressible Euler equations:

$$\begin{aligned} &(\partial_t + U\partial_x)u + v\partial_z U = -\partial_x p, \\ &(\partial_t + U\partial_x)v = -\partial_z p, \\ &\partial_x u + \partial_z v = 0. \end{aligned} \tag{19}$$

The incompressibility condition allows the introduction of the stream function ψ such that

$$u = \partial_z \psi, \qquad v = -\partial_x \psi. \tag{20}$$

We are interested in disturbances which propagate in the mean flow direction and take the form of spatio-temporal waves, i.e.,

$$\psi(x,z,t) = \mathrm{Re}\big[\phi(z)\exp\{\mathrm{i}(kx-\omega t)\}\big], \tag{21}$$

where Re denotes the real part. Substituting the expressions (20) and (21) into the momentum equations of (19), one obtains the standard Rayleigh equation

$$\left(U - \frac{\omega}{k}\right)(\phi'' - k^2\phi) - U''\phi = 0, \tag{22}$$

where a prime denotes differentiation with respect to z. The boundary conditions are given by

$$\lim_{z\to\pm\infty} \phi(z) = 0. \tag{23}$$

The pressure distribution takes the normal mode form

$$p(x,z,t) = \mathrm{Re}\big[\,\widehat{p}(z)\exp\{\mathrm{i}(kx-\omega t)\}\big], \quad \text{with } \widehat{p} = U'\phi - \left(U - \frac{\omega}{k}\right)\phi'. \tag{24}$$

It is shown in [18] that for the Rayleigh equation and the hyperbolic tangent velocity profile at $R = 1$, the possible instabilities are convective. We then consider only real angular frequencies ω and complex wave numbers $k = k_r + \mathrm{i}k_i$. The spatial growth rate is $-k_i$ and the phase velocity ω/k_r. Michalke [16] has solved this problem numerically and the resulting phase velocity and spatial growth rate are given in Fig. 8. The most amplified perturbations are obtained for a Strouhal number of 0.0329.

4.2. Links with experiments

The previous theoretical results, phase velocity and spatial growth rate, are compared with the quantities which can be extracted from the pressure measurements along the neck.

4.2.1. Convection velocity

Convection velocity measurements in turbulent shear flows have been discussed by Wills [28]. Here, the convection velocity is obtained through the phase angle φ between the coherent pressure signals p_1, p_2 and p_3 as

$$U_c = \omega_c L/\varphi, \tag{25}$$

where the ratio φ/ω_c represents the duration taken by the perturbation to cross the neck length. It should be noticed that the phase angle is always measured *modulo* 2π which may lead to an ambiguity. In the present case, it is assumed that there is only one fundamental period involved in the resonance problem and this ambiguity vanishes.

Using the phase angle between the trailing and the leading-edge $\varphi_{2/1}$ given in Fig. 6, we obtain the results shown in Fig. 8 where they are compared with the theoretical values. The agreement is seen to be very good.

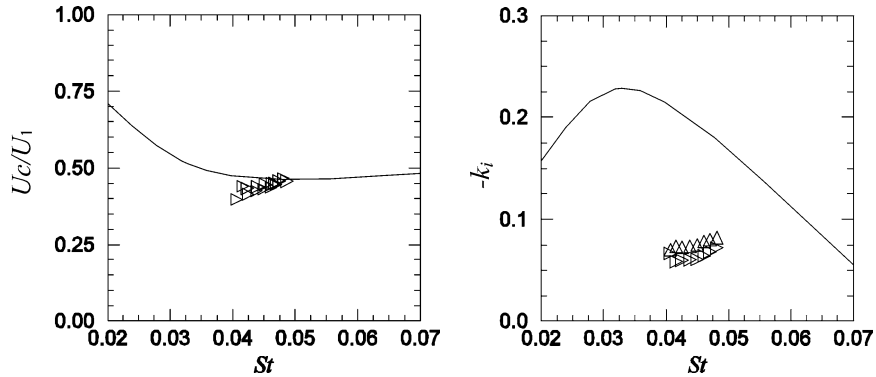

Fig. 8. Phase velocity U_c/U_1 and spatial growth rate $-k_i$ versus Strouhal number St: —, Michalke [16]; ▷, experiments using p_1/p_2; Δ, experiments using p_3/p_2.

4.2.2. Pressure in the neck

Starting from the wall pressure measurements, a rough estimation of the growth rate $-k_i$ can be obtained, by fitting the experimental pressure levels with the exponential distribution (24) of the shear layer pressure. The measurements are performed in presence of cavity resonance. This leads to the data shown in Fig. 8 where the comparison with the theoretical values is seen to be unsatisfactory.

The disagreement is partly due to the reference length L_0 defined at 50% of the neck length which is, in reality, not constant along the stream, leading to continuously changing value of the experimental Strouhal number. Ho and Huerre [29] among others, have shown that a turbulent mixing layer spreads linearly along the mean flow direction, with a spreading rate $\mathrm{d}L_0/\mathrm{d}x = 0.09$ for a velocity ratio $R = 1$. By applying this linear evolution and by taking the value at 75% of the neck length as a more representative median value, the corrected reference length becomes $L_0^* = 1.25L_0$. This correction applies also on the Strouhal number and we observe then that the experimental results get closer to the theoretical results. It should be noticed that the convection velocity might be corrected in the same way, without changing the good agreement between theory and experiments, since it is almost constant in this region.

Even with this correction, the agreement for the growth rate is not satisfactory. As pointed out by Michalke [16], nonlinear effects which are intensified by the cavity are not accounted for in the theory. In the present case, it is not surprising that the shear layer in the neck, forced by the cavity resonance, produces a flatter pressure distribution, such as the one created by a piston, rather than the exponential distribution of a free shear layer.

It is obvious that our shear layer is saturated by resonance with the cavity acoustics. In the cavity problem, the interactions with the neck lips and the cavity volume are crucial and these phenomena are not taken into account in the framework of classical linear stability theory, as pointed out by Rockwell [21]. The limitations of linear stability theory can be illustrated by observing the resonance frequency evolution with velocity.

4.3. Frequency evolution

The measured Strouhal number is plotted versus free-stream velocity U_1 in Fig. 9. The cavity reduced frequency and Rossiter's Strouhal number are also displayed. Resonance occurs when these curves cross.

The Rossiter formula [2] is commonly used in order to obtain the frequencies generated in a shear layer developing in a neck. It includes the feed-back mechanism but not the interaction with the cavity volume. A discussion of this formula has been given by Tam and Block [3] and more recently in [30,5]. In our case, it is given by

$$St\frac{L}{L_0} = \frac{n-\gamma}{M + U_1/U_c}, \tag{26}$$

where n is an integer characterizing the order of the mode. In this paper we have $n = 1$ due to the physical dimensions of the set-up. The empirical parameter γ, linked to the shape of the neck lips and the cavity depth, represents the phase lag in the feed-back loop. In the usual scenario, the corresponding time delay γ/f is the sum of the times taken for the impingement of a vortex at the trailing edge, emission of an acoustic pulse, arrival of the pulse at the leading edge and finally shedding of a new vortex.

We already have measured the convection velocity in the previous section. The value of γ can now be estimated as 0.090 which is approximately 3 times lower than the value 0.25 proposed by Rossiter. This difference is attributed to the very low

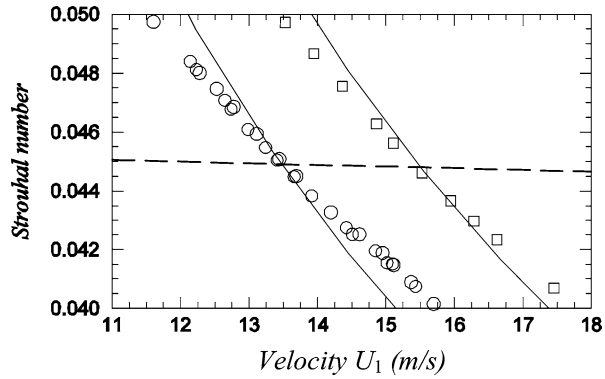

Fig. 9. Strouhal number versus free-stream velocity U_1: —, cavity reduced frequency; - - -, Rossiter's formula; ○, measurements cavity A; □, measurements cavity B.

Mach number flow ($M = 0.04$ at resonance) which makes the compressibility effect negligible in the feed-back mechanism. There is also the interaction with the cavity neck, with a neck length much lower than the acoustic wavelength, which should probably be taken into account [30].

Coming back to Fig. 9, one can observe that the measurements do not follow those of any single oscillator, cavity or shear layer. When the free-stream velocity U_1 is varied outside the range displayed in Fig. 9, the system is off resonance and due to a poor signal-to-noise ratio the frequency of the shear layer and the frequency of the cavity mode can be observed separately but not correctly measured.

5. Sound reduction

This section is devoted to the description of a forcing technique of the shear layer, the purpose of which is the reduction of the pressure level in the cavity. In a first step we present the experiments and in a second step, a deeper analysis of the results is made.

5.1. Experiments

5.1.1. Actuators

The noise reduction setup is mounted on the surface of the upstream lip. It consists of a series of small flaps which are constituted of piezo-electric material. Such a technique has already been used, for instance in [12,13]. Our setup differs however in the sense that our flaps are discontinuously distributed along the span of the neck, as shown in Figs. 10 and 11.

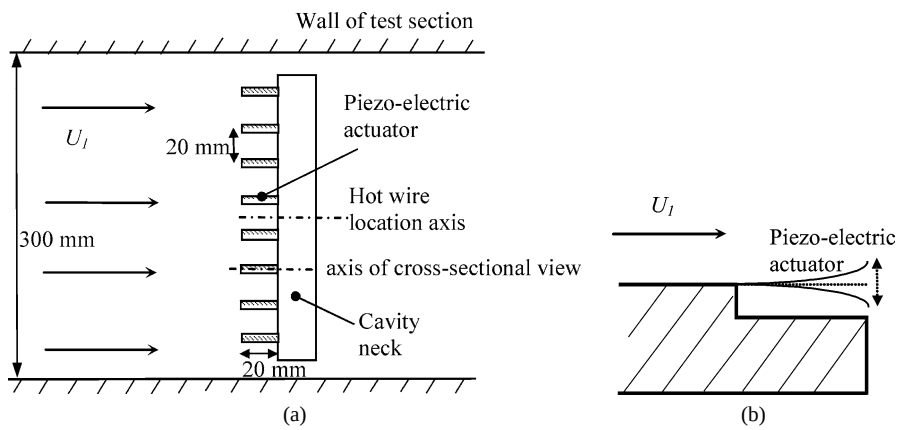

Fig. 10. Actuators mounting: (a) top view; (b) cross-sectional view of upstream lip region.

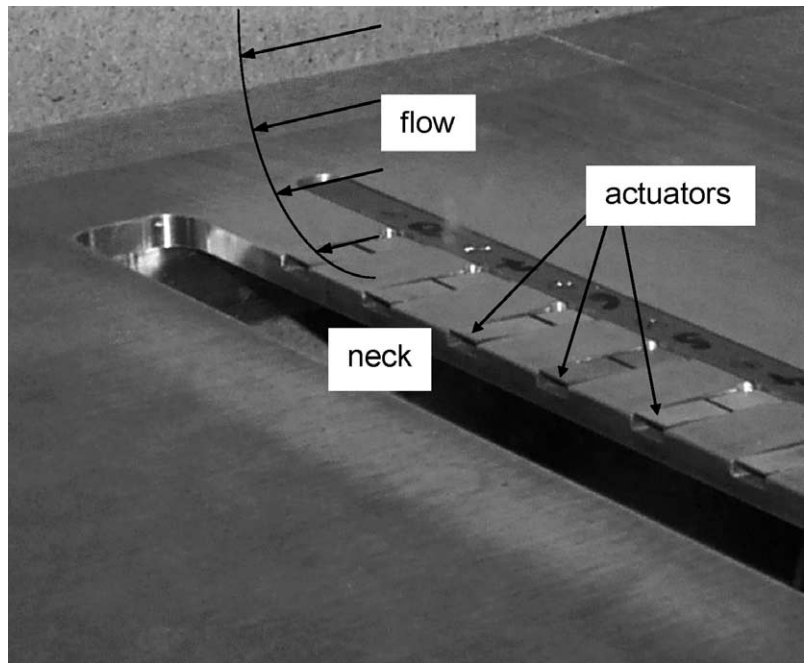

Fig. 11. Photo of the cavity neck and the actuators at the upstream lip.

The actuators are piezo-electric bimorph elements (two layers of PZT with a middle layer metal sheet, provided by Piezomechanik) which are assembled in order to produce a bending motion as in a cantilever beam. Their active length is 20 mm, and their width 6 mm, which leads to a bending eigenfrequency in the desired range, around 310 Hz. Eight actuators are mounted spanwise with a distance of 20 mm between their axis. This distance represents one length wave in the neck, and it is expected that it is small enough to be efficient.

These actuators are all excited electrically by the same sine signal at a frequency of 310 Hz. This value is their first bending frequency, for which the obtained displacement is maximum. All the actuators are correlated, i.e. they are all in phase. An arbitrary estimate of the displacement amplitude gave an order of magnitude of ± 0.25 mm at their extremity. It is expected that the perturbation produced is almost two dimensional, as if the actuators were a unique large flap. There is also the possibility to use only one actuator out of two, in order to have an estimate of the influence of spanwise separating distance.

This system does not contain any feedback loop and may not qualify as an active control scheme, as for instance in [11]. We have however to bring an external energy into the system. Our purpose here is to propose a simple forcing technique rather than a comprehensive active control scheme.

5.1.2. Results

The results are presented in Table 4 for the two cavity A resonance peaks and the cavity B single resonance. Pressure levels are extracted from a power spectral density function in $\mathrm{Pa}/\sqrt{\mathrm{Hz}}$. Typical spectra are plotted in Fig. 12 for the cavity A first peak. The thin peak at 310 Hz in the spectrum with actuators on corresponds to a vibroacoustic perturbation of the microphone, occurring also without wind and must be considered as an experimental artefact.

The sound reduction is observed to be very efficient for cavity A and the technique seems to work simply by detuning of the resonance frequency. The case of cavity B reinforces this interpretation: the actuators are indeed forcing the shear layer at its natural resonance with the cavity, leading as expected to a higher level of the cavity pressure. The residual noise for cavity A is

Table 4
Cavity pressure levels without and with the sound reduction scheme

Number of actuators	Cavity A peak 1	Cavity A peak 2	Cavity B
0	24.5	28.3	49.4
4	8.4	–	–
8	1.4	2.1	95.0

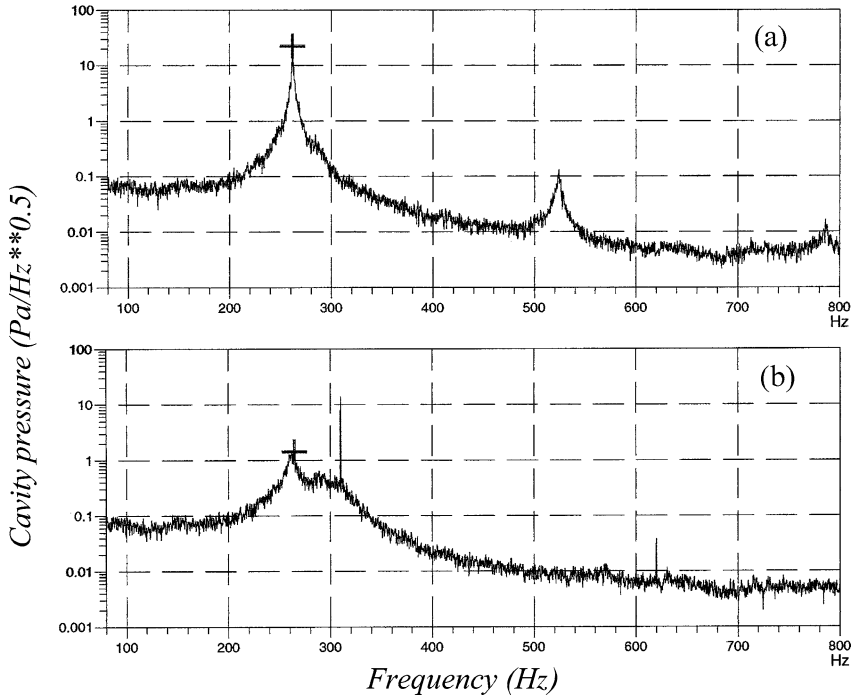

Fig. 12. Power spectral density of cavity pressure p_v at resonance: (a) without forcing; (b) with forcing at 310 Hz.

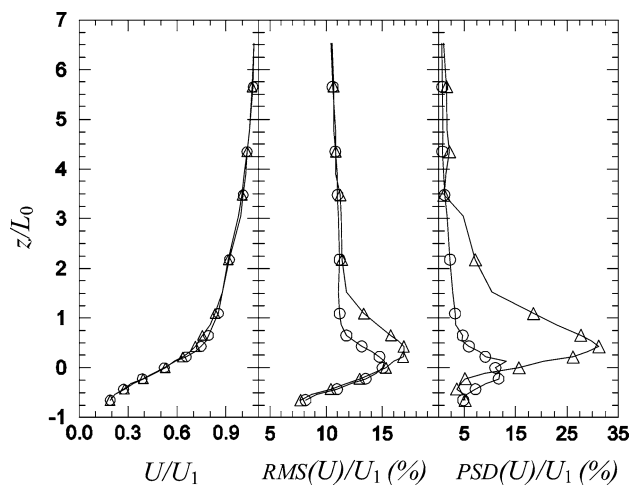

Fig. 13. Shear layer velocity profiles at $x = 0.5L$: ○, free unforced case; △, forced case.

close to that of turbulence when all the actuators are on. When only one out of two actuators is on, the sound is reduced but a nonnegligible sound level remains.

The shear layer velocity profiles with forcing have been measured and plotted in Fig. 13 where they are compared with the free unforced case. The mean velocity profile is not perturbed by the actuators and remains identical as in the natural case. Cattafesta et al. [12] also found the same behaviour. This implies that the cavity drag is not modified: a confirmation was obtained by measuring the mean pressure inside the cavity which did not show any difference without and with the actuators on.

The unsteady part of the shear layer is however considerably modified as seen in Fig. 13 for the root-mean-square (RMS) level. The latter results from the integration of a large frequency band and is not representative of what really happens at the frequency of interest. This has led us to extract the single resonance or forcing frequency component by means of the power spectral density (PSD), that is 262 Hz for the free case and 310 Hz for the forced case. It is seen in Fig. 13 that the actuators

provide a larger component than in the unforced case (ratio around 2.5). Forcing also induces the maximum amplitude to be located at a higher vertical position which is a consequence of the geometrical design of the actuators, flush mounted on the upstream wall.

5.2. Discussion

In these experiments, the technology of the actuators allows us to explore the effect of a single control frequency. The limitations of the sound reduction scheme cannot be obtained experimentally but these can be estimated with the help of hydrodynamic stability theory, as shown below.

The idea is to deal with a characteristic quantity, such as an energy ratio, corresponding to the spatial mean square pressure in the neck. The reference energy is chosen at natural resonance. Starting from the pressure distribution (24), we define the energy ratio as

$$\chi = \left(\frac{\int_0^L \exp[-k_{ic}x]\,\mathrm{d}x}{\int_0^L \exp[-k_i x]\,\mathrm{d}x} \right)^2, \tag{27}$$

where $-k_{ic}$ is the spatial growth rate corresponding to resonance and $-k_i$ is the spatial growth rate associated with the forcing control frequency. Thus $1/\chi$ represents the relative energy necessary to overcome the natural resonance of the system. In other words, it is a measure of the forcing energy required for the control to be effective at the particular forcing Strouhal number under consideration. The parameter χ is plotted in Fig. 14 for the natural resonance observed in the experiments (solid curve) and for the theoretical case (dashed curve) where the resonance would occur at the maximum growth rate in Fig. 8. The Strouhal number St^* is the one obtained with the corrected reference length L_0^* as in Section 4.2.2. The double arrow indicates the forcing Strouhal number used experimentally for cavity A peak 1.

Consider first the experimental curve $\chi(St^*)$: when the forcing Strouhal number coincides with the resonance frequency $St^* = 0.056$, $\chi = 1$ since $-k_i = -k_{ic}$. As the forcing Strouhal number is increased above the resonance value, χ increases above unity since $-k_i < -k_i$ (see Fig. 8): controlling the resonance becomes "harder and harder" in the sense that a larger amount of forcing energy is required. As the forcing Strouhal number is decreased below the resonance value, χ decreases below unity since $-k_i > -k_{ic}$: controlling the flow is "cheaper". This trend persists as long as the forcing Strouhal number is larger than the Strouhal number of maximum growth rate. As St^* is further decreased, the control energy starts to rise again since $-k_i$ takes smaller and smaller values.

The same reasoning applies for the dashed curve: $\chi = 1$ when St^* coincides with the Strouhal number of maximum growth rate which is assumed to be resonant. As St^* departs from this resonance point, from above or from below, χ increases above unity and effective control requires a gradually larger forcing energy.

The velocity component displayed in Fig. 13, raised to the fourth power in order to represent the energy indicates that the actuators provide an energy which is about 40 times larger than in natural resonance. This much more than required in comparison with the ratio 1.8 computed in Fig. 14.

We have already mentioned the limitations of linear stability theory concerning the lock-in mechanism. The current interpretation has to take this feature into account: there is a small region surrounding the resonance frequency where the forcing will enhance the instability, a feature which is not accounted for in the definition of χ. This is precisely what happens with cavity B where only a feedback control would be efficient.

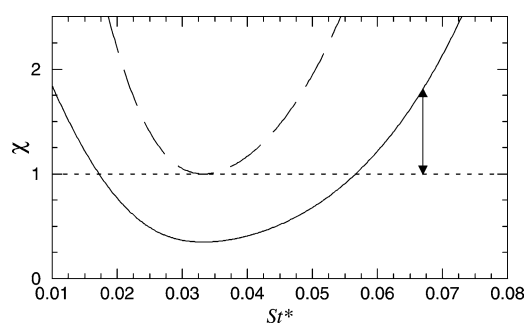

Fig. 14. Energy amplitude ratio χ from (27) for control versus corrected Strouhal number St^*: —, present case; - - -, at maximum growth rate. Double arrow indicates experimental forcing Strouhal number.

6. Conclusion

A study of the pressure oscillations generated by a low-speed flow over a deep cavity has been presented. The thread of the paper is to provide a justification for a resonance reduction scheme based on detuning the frequency of the unstable impinging shear layer from the cavity mode frequency. The shear layer forcing technique is rather simple and does not modify the mean flow characteristics.

If mounted on a car sunroof, it should not increase the mean drag coefficient, as in the case of the usual spoilers. Active spoilers can then be designed using the Strouhal number as the main similarity parameter. These spoilers could be discrete as in the present study, but one can expect that a unique two dimensional spoiler would probably be easier to implement. Due to the very low frequencies involved in a passenger cabin, the piezo-electric actuators can be replaced by standard electro-magnets which are more reliable. The improvement of the instrumentation in recent generations of car vehicles allows the excitation signal to be set easily by the vehicle speed, using the linear law provided by the Strouhal similarity.

The method and its limitations have been discussed in light of classical linear stability analysis. More investigations are required in order to develop a nonlinear model which should be capable of reproducing the real behaviour of the coupled cavity-shear layer system.

Acknowledgements

The authors wish to express warm thanks to Prof. P. Huerre for the stimulating discussions and his contribution to the improvement of the manuscript.

References

[1] S.W. Kang, J.M. Lee, S.H. Kim, Structural-acoustic coupling analysis of the vehicle passenger compartment with the roof, air-gap and trim boundary, ASME J. Vib. Acoust. 122 (2000) 196–202.
[2] J.E. Rossiter, Wind tunnel experiments on the flow over rectangular cavities at subsonic and transonic speeds, Aero. Research Council Reports and Memoranda, Technical Report 3438, 1964.
[3] C.K.W. Tam, P.J.W. Block, On the tones and pressure oscillations induced by flow over rectangular cavities, J. Fluid Mech. 89 (1978) 373–399.
[4] M.J. Lucas, R. Noreen, L.D. Sutherland, J. Cole III, M. Junger, The acoustic characteristics of turbomachinery cavities, NASA CR 4671, 1995.
[5] C.W. Rowley, T. Colonius, A.J. Basu, On self-sustained oscillations in two-dimensional compressible flow over rectangular cavities, J. Fluid Mech. 455 (2002) 315–346.
[6] L.F. East, Aerodynamically induced resonance in rectangular cavities, J. Sound Vib. 3 (1966) 277–287.
[7] R.L. Panton, Effect of orifice geometry on helmholtz resonator. Excitation by grazing flow, AIAA J. 28 (1) (1990) 60–65.
[8] P.J. Disimile, N. Toy, E. Savory, Effect of planform aspect ratio on flow oscillations in rectangular cavities, ASME J. Fluids Engrg. 122 (2000) 32–38.
[9] H. Kook, L. Mongeau, D.V. Brown, S.I. Zorea, Analysis of interior pressure oscillations induced by flow over vehicle openings, Noise Control Engrg. J. 45 (6) (1997) 223–234.
[10] M. Sunyach, J.-C. Bera, Active control of flow instabilities generated by cavities, in: VKI Lecture Ser., vol. 1997-07, 1997.
[11] H. Kook, L. Mongeau, M.A. Franchek, Active control of pressure fluctuations due to flow over Helmholtz resonators, J. Sound Vib. 255 (1) (2002) 61–76.
[12] L.N. Cattafesta III, S. Garg, M. Choudhari, F. Li, Active control of flow-induced cavity resonance, AIAA paper 97-1804, 1997.
[13] S. Kikushi, Y. Fukunishi, Active flow control technique using piezo-film actuators applied to the sound generation by a cavity, ASME paper FEDSM99-7232, 1999.
[14] X. Amandolese, P. Hemon, F. Santi, J. Wojciechowski, Réduction semi-active du battement de volume engendré par une cavité profonde soumise à un écoulement aérodynamique, C. R. Mécanique 330 (2002) 101–106.
[15] A. Michalke, On the inviscid instability of the hyperbolic-tangent velocity profile, J. Fluid Mech. 19 (1964) 543–556.
[16] A. Michalke, On spatially growing disturbances in an inviscid shear layer, J. Fluid Mech. 23 (1965) 521–544.
[17] P.A. Monkewitz, P. Huerre, Influence of the velocity ratio on the spatial instability of mixing layers, Phys. Fluids 25 (7) (1982) 1137–1143.
[18] P. Huerre, P.A. Monkewitz, Absolute and convective instabilities in free shear layers, J. Fluid Mech. 159 (1985) 151–168.
[19] C.-M. Ho, L.-S. Huang, Subharmonics and vortex merging in mixing layers, J. Fluid Mech. 119 (1982) 443–473.
[20] S. Ziada, D. Rockwell, Oscillations of an unstable mixing layer impinging upon an edge, J. Fluid Mech. 124 (1982) 307–334.
[21] D. Rockwell, Oscillations of impinging shear layers, AIAA J. 21 (5) (1983) 645–664.
[22] M. Meissner, Aerodynamically excited acoustic oscillations in cavity resonator exposed to an air jet, Acta Acoustica united with Acustica 88 (2002) 170–180.
[23] M. Bruneau, Manuel d'acoustique fondamentale, Hermès, Paris, 1998.

[24] D.G. Crighton, A.P. Dowling, J.E. Ffowcs Williams, M. Heckl, F.G. Leppington, Modern Methods in Analytical Acoustics, 2nd edition, Springer-Verlag, London, 1994.
[25] X. Amandolese, P. Hemon, C. Regardin, A study of the acoustic oscillations by flows over cavities, ASME J. Vib. Acoust. (2002), submitted for publication.
[26] H.R. Graf, W.W. Durgin, Measurement of the nonsteady flow field in the opening of a resonating cavity excited by grazing flow, J. Fluids Structures 7 (1993) 387–400.
[27] P. Huerre, M. Rossi, Hydrodynamic instabilities in open flows, in: C. Godrèche, P. Manneville (Eds.), Hydrodynamics and Nonlinear Instabilities, Cambridge University Press, Cambridge, 1998.
[28] J.A.B. Wills, On convection velocities in turbulent shear flows, J. Fluid Mech. 20 (1964) 417–432.
[29] C.-M. Ho, P. Huerre, Perturbed free shear layers, Ann. Rev. Fluid Mech. 16 (1984) 365–424.
[30] X. Gloerfelt, Bruit rayonné par un écoulement affleurant une cavité : simulation aéroacoustique directe et application de méthodes intégrales. Ph.D. Thesis of École Centrale de Lyon, France, 2001.